Thermal conductivity of nitrogenated ultrananocrystalline diamond films on silicon

M. Shamsa,[1,a)] S. Ghosh,[1] I. Calizo,[1] V. Ralchenko,[2] A. Popovich,[2] and A. A. Balandin[1,3,b)]
[1]*Nano-Device Laboratory, Department of Electrical Engineering, University of California-Riverside, Riverside, California 92521, USA*
[2]*A.M. Prokhorov General Physics Institute of the Russian Academy of Sciences, Moscow 119991, Russia*
[3]*Materials Science and Engineering Program, Bourns College of Engineering, University of California-Riverside, Riverside, California 92521, USA*

(Received 7 August 2007; accepted 19 February 2008; published online 24 April 2008)

The authors report on the experimental investigation of the thermal conductivity of nitrogenated ultrananocrystalline diamond (UNCD) films on silicon. For better accuracy, the thermal conductivity was measured by using two different approaches: the 3ω method and transient "hot disk" technique. The temperature dependence of the thermal conductivity of the nitrogenated UNCD films was compared to that of undoped UNCD films and microcrystalline diamond (MCD) films on silicon. It was shown that the temperature dependence of the thermal conductivity of UNCD films, which is substantially different from that for MCD films, can be adequately described by the phonon-hopping model. The room-temperature thermal conductivity of UNCD is 8.6–16.6 W/m K and decreases with the addition of nitrogen. The obtained results shed light on the nature of thermal conduction in partially disordered nanostructured materials and can be used for estimating the thermal resistance of doped UNCD films. © *2008 American Institute of Physics*. [DOI: 10.1063/1.2907865]

I. INTRODUCTION

A wide variety of carbon-based materials, including diamond, polycrystalline diamond (PCD), diamondlike carbon (DLC), carbon nanotubes, and single-layer graphene, have recently attracted attention as possible candidates for beyond-silicon (Si) complementary metal-oxide-semiconductor electronic device applications. Diamond has a number of exceptional properties, such as tremendous hardness, chemical inertness, record high thermal conductivity, high mobility of charge carriers, and high electron emission at low fields.[1–3] These properties have already made diamond a material of choice for wear-resistive coatings, optical windows, surface acoustic-wave devices, heat spreaders, and field-emission flat panel displays. More recently, there has been noticeable progress with the low-temperature deposition and doping of diamond.[1,2,4,5]

Nanocrystalline diamond (NCD) films have been successfully synthesized at a low temperature and at a relatively high growth rate.[6–9] While conventional microcrystalline diamond (MCD) films are grown in an essentially hydrogen-rich atmosphere, NCD films can be produced in gas mixtures with low (or even zero) H_2 addition to the plasma.[6] NCD films, which are synthesized by the argon-rich microwave plasma assisted chemical vapor deposition (MPCVD) process, can have a grain diameter as small as $d \sim 2-5$ nm. Such films are also referred to as ultrananocrystalline diamond (UNCD). The important benefit of UNCD films on Si substrates compared to that of faceted MCD films is that UNCD films are smooth pinhole-free, even for very small thicknesses W, e.g., $W \ll 1$ μm. It has also been demonstrated that the electrical conductivity of UNCD films can be changed by the addition of nitrogen (N_2) in the process gas, which leads to the formation of a n-type material.[8,10,11] Low electrical contact resistance and ability to form Ohmic contacts were reported in Refs. 12 and 13. DLC was used to substitute for the buried SiO_2 layer in silicon on insulator,[14] while carbon layers were utilized in the deep trench dynamic random access memory cell.[15] At the same time, the most important application of UNCD materials is in microelectromechanical and nanoelectromechanical systems due to their mechanical and frictional properties, which are similar to those of diamond.[16]

While the addition of nitrogen and the resulting electrical conductivity are important for the proposed electronic or field-emission applications of UNCD, one should also understand how the thermal conductivity (K) of UNCD is different from that of crystalline diamond and MCD films, in particular, if carbon materials are used to mitigate the device self-heating problems.[14] Thus, the effect of nitrogen addition on the thermal conductivity of UNCD films is also of major interest. In its bulk single crystal or polycrystalline forms, diamond has the highest thermal conductivity among all materials, which at room temperature (RT) is $K = 1000-2200$ W/m K, depending on the quality.[17–20] The thermal conductivity of NCD and UNCD films is much smaller. Although only limited work has been published on the thermal conductivity of NCD and UNCD, one can notice a substantial discrepancy due to the differences in the material properties and measurement techniques. The RT values reported for these materials vary from $K \sim 12$ W/m K[21] to $K \sim 26$ W/m K.[22] Some of us reported the first study of the thermal conductivity temperature dependence in UNCD films.[23] Since the thermal conductivity of carbon-based materials strongly depends on the microcrystalline structure as

a)Present address: Intel Corporation, Hillsboro, OR 97124.
b)Author to whom correspondence should be addressed. Electronic mail: balandin@ee.ucr.edu. URL: http://www.ndl.ee.ucr.edu/.

well as phase and the amount of the sp^2/sp^3 disorder,[24] one should make a special effort to accompany the thermal study with a detailed structural characterization of the samples and correlate the K values with the material structure.

In this paper, we report the experimental study of the thermal conductivity of nitrogenated UNCD films on Si by using two different measurement techniques: the 3ω and the "hot disk." Due to the difficulties associated with the measurements of the thermal conductivity of thin-film samples, it is important to validate the results by applying more than one experimental technique. The application of the two experimental techniques has also allowed us to minimize the system error in the thermal conductivity measurements, which often lead to a data discrepancy. The samples used for the thermal conductivity study were rigorously characterized by optical microscopy, transmission electron microscopy, scanning electron microscopy (SEM), x-ray diffraction (XRD), and micro-Raman spectroscopy. For comparison, we also studied undoped UNCD and MCD films on Si. The experimental results were interpreted by using the phonon-hopping model.[25]

II. SAMPLE PREPARATION AND CHARACTERIZATION

The samples were grown on Si substrates in a MPCVD reactor (model DF-100, 2.45 GHz). The MCD film that was used as a reference in our study had a thickness of 3.4 μm and a surface roughness $R_a=133$ nm. The MCD film (also referred to as polycrystalline or "poly") was grown for 2 h with a gas mixture of 4% CH_4/96% H_2 at a substrate temperature of $T=800$ °C, a pressure of 90 Torr, and a microwave power of 4.3 kW. The UNCD samples UNCD-0 ($W=2.2$ μm), UNCD-15 ($W=8.9$ μm), and UNCD-25 ($W=9.5$ μm) were grown in the same CVD reactor by using Ar-rich gas mixtures Ar/(5%) H_2/(2%) CH_4/N_2 with N_2 concentrations of 0%, 15%, and 25%, respectively. Ar was varied to balance the total flow rate of 500 SCCM (SCCM denotes cubic centimeter per minute at STP) at the following conditions: microwave power of 2.4 kW, pressure of 90 Torr, and substrate temperature $T=800$ °C.

The surface morphology of the undoped (UNCD-0 sample) film is shown on the SEM image in Fig. 1(a). The small (7–10 nm) grains form larger aggregates of 40–70 nm size. The average surface roughness R_a for the UNCDs was below 40 nm, as measured by atomic force microscope. One should note that no columnar growth features have been observed in the film cross section [Fig. 1(b)]. In contrast, the MCD film showed a typical feature for the polycrystalline CVD diamond columnar grain structure, which was clearly seen in the cross sections produced by the cleavage. The grain size on the growth side was close to 2 μm, as evaluated from the SEM images.

The XRD analysis (JDX-10P instrument, JEOL) of all UNCD samples revealed the presence of the cubic diamond phase with a lattice parameter $a=0.35663$ (± 5) nm, as found from the (200) reflex position. The grain size $d=17-26$ nm was determined for the UNCD films from the XRD data[26] by using Scherrer's formula for the (111) reflex broadening. These XRD-derived d values, which are larger than the apparent particle sizes seen in the SEM images, were used in the further analysis of the phonon transport.

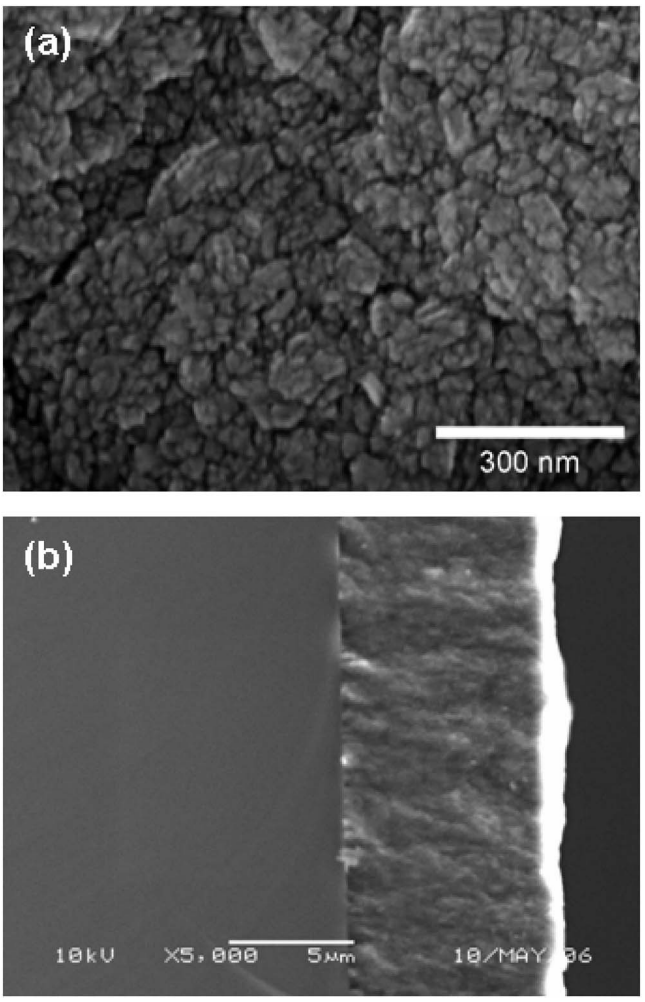

FIG. 1. (a) SEM plan view image of the ultrananocrystalline film without added N_2; (b) SEM image of the cross section of UNCD film grown on the Si substrate with 15% N_2 added in gas. The substrate is on the left.

It is important to verify the morphology, sp^2/sp^3 content, and microstructure of the grown films. Micro-Raman spectroscopy was used to accomplish this task. The RT Raman spectra of UNCD and MCD films were obtained by using a Renishaw spectrometer fitted with an argon ion (Ar^+) visible 488 nm laser and a grating with a groove density of 1800 lines/mm. An optical path through the 50× objective of an optical microscope was used for both the light collection and the delivery (180° backscattering configuration). The Raman spectra were collected from 800 to 3000 cm^{-1} for 10 s and accumulated ten times. Figure 2(a) shows the Raman spectra of three distinctively different types of carbon materials, i.e., natural crystalline diamond, highly oriented pyrolytic graphite (HOPG), and MCD, which were used for comparison to UNCD. In the MCD film, the most pronounced peak is at 1332 cm^{-1} with a full width at half maximum of 10 cm^{-1}, which corresponds to the optical vibrations in sp^3-bonded carbon atoms in the diamond crystal structure, while a weak peak at 1500 cm^{-1} is associated with an sp^2-dominant disordered carbon.[27,28] Figure 2(a) also shows the spectra for the reference HOPG and single crystal bulk

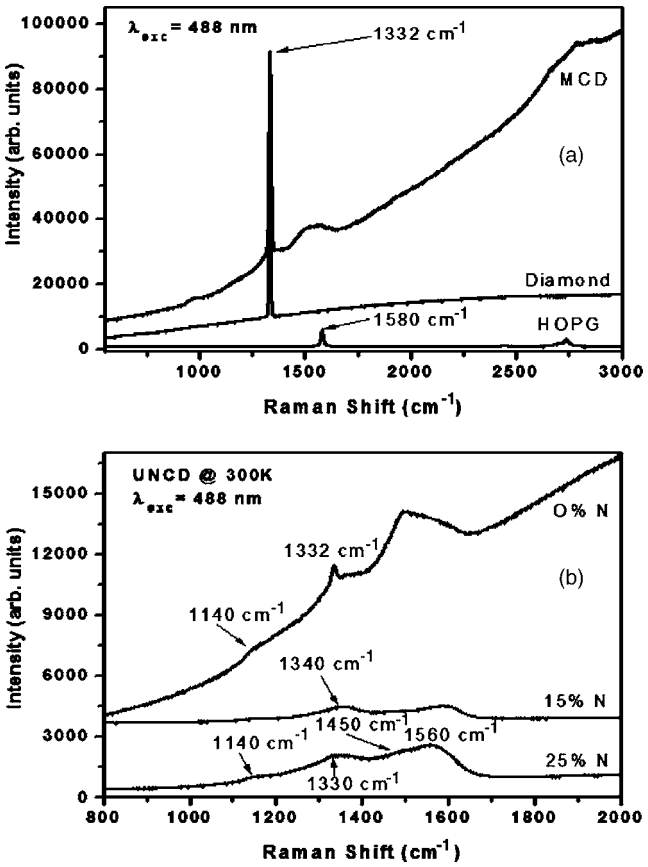

FIG. 2. Raman spectra from the (a) MCD, crystalline diamond, and HOPG graphite samples and (b) UNCD diamond films with 0%, 15%, and 25% nitrogen contents.

diamond samples. In the HOPG spectra, there are two prominent peaks. The G peak at 1580 cm^{-1} arises from the zone center E_{2g} phonon in graphite,[29] while the 2D band at around 2700 cm^{-1} is due to second order zone boundary phonons resulting in the two subpeaks, $2D_1$ and $2D_2$, at 2695 and 2737 cm^{-1}, respectively.[30] For the diamond sample, we observe its zone center optical phonon at 1332 cm^{-1}, which coincides with the aforementioned peak in the MCD film.

The Raman spectra of the undoped and nitrogenated UNCD films are shown in Fig. 2(b). They are markedly different from the spectra of other phases of carbon. The peaks that are observable in the UNCD samples are at 1140 and 1330 cm^{-1} and the overlapping peaks at 1450 and 1560 cm^{-1}. The origin of the peaks at 1140 and 1450 cm^{-1} is attributed to the sp^2 phase in the *trans*-polyacetylene segments at the grain boundaries.[31,32] The peaks at ~1330 and 1560 cm^{-1} are the D and G bands, respectively, which are associated with the sp^2-bonded carbon at the grain boundaries.[33,34] It has been noted that the broadening of the D band is due to the decreasing of the grain size from the micro- to nanometer scale.[35] With the addition of N_2, the sp^2 clusters become larger and, consequently, we observe that the intensity of the D band decreases, while the intensity of the G band increases.[36,37] The Raman spectra of our UNCD samples under UV excitation at 244 nm have been reported by some of us elsewhere.[38] The UV-excited spectra manifested a clear diamond peak at 1333 cm^{-1} both in the undoped and the nitrogenated films with a tendency of the G peak of graphite to increase with the nitrogen amount in the plasma.

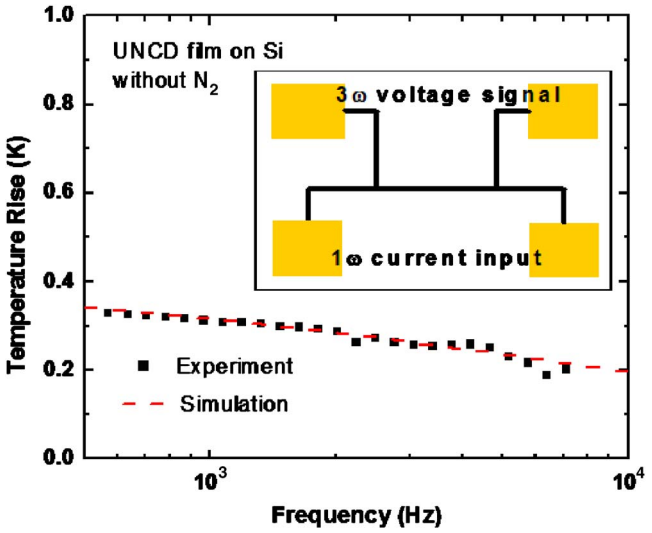

FIG. 3. (Color online) Measured (symbol) and simulated (dash) temperature rises as a function of frequency at 300 K for the UNCD sample without nitrogen. The inset shows the schematic of the 3ω heater/thermometer element photolithographically patterned on top of the UNCD sample.

III. EXPERIMENTAL DETAILS

Reported data for thermal conductivity of thin films often show discrepancies due to the systematic errors of a particular measurement technique. For this reason, we measured the thermal conductivity by using two different methods. The first one is the 3ω ("3-omega") method.[39] The second method is the transient plane source (TPS) technique carried out with a Hot Disk, AB instrument. Below, we describe the measurement procedure for each technique in more detail.

A. Thermal conductivity measurements by the 3ω method

The 3ω thermal conductivity measurement technique is based on driving an ac through a metal line placed on top of the sample under investigation (see inset of Fig. 3). This metal conductor simultaneously acts as a heater and as a thermometer.[39,40] Driving an ac through the heater/thermometer at a frequency 1ω results in a measurable electrical resistance change at a frequency of 3ω due to the heating of the metal conductor. The amplitude of the temperature oscillations, which is measured through the resistance change, depends on the power input, frequency, and physical properties of the material under the heater/thermometer, such as the thermal conductivity K, mass density ρ, and heat capacitance C_V. Since the nitrogenated UNCD films were electrically conductive (the measured electrical resistivity is $\sim 3 \times 10^{-2}$ Ω cm for the strongly nitrogenated UNCD-25 sample[41]), we had to insulate them from the heater-thermometer line. For this purpose, a 90 nm thick SiN insulation layer was deposited on the top surfaces by plasma-enhanced chemical vapor deposition (PECVD) to provide the electrical insulation. A Si reference sample with an identical

PECVD deposited SiN insulation layer was prepared for the data subtraction in the differential 3ω technique. The differential 3ω technique allowed us to separate the thermal conductivity of the UNCD films from the overall thermal resistance of the film under study and the electrical insulation layer. The thermal diffusion depth $\delta_T=(\alpha/2\omega)^{1/2}$ (where α is the thermal diffusivity) was controlled via selection of the proper frequency range.

Cr (10 nm)/Au (100 nm) metallic heater/thermometer wires with widths of 10 and 30 μm were patterned on top of the insulation layer on each of the samples by photolithography, which was followed by e-beam evaporation and the lift-off process. The 3ω thermal conductivity measurements over the temperature range from 80 to 400 K were conducted inside a Janis ST-300 vacuum cryostat by using the home-built experimental setup. A lock-in amplifier was used to provide the first harmonic input power and collect the harmonic temperature rise signals from the sample.[42,43] Figure 3 shows the measured temperature rise as a function of frequency in the "undoped" UNCD film at 300 K. The simulated temperature rise, which is obtained from the heat diffusion equation, is also shown with the dashed line.

B. Thermal conductivity measurements by the hot disk technique

The transient plane source (TPS) technique, which is also referred to as the hot-disk technique,[44] utilizes the TPS element, which serves as a heat source as well as the temperature sensor. The TPS is a thin layer of a bifilar spiral pattern made of an electrically conducting material, such as Ni. The pattern is covered with a layer of Kapton to provide electrical insulation for measurement of conductive samples. During the experiment, the sensor is sandwiched between the two samples and heated by the short current pulse. The heating is measured as a voltage change of the sensor element.

The transient resistance change $R(t)$ caused by the temperature oscillations is given as[44] $R(t)=R_0[1+\beta\overline{\Delta T(\tau)}]$. Here, R_0 is the initial resistance of the sensor before the current pulse is applied, β is the temperature coefficient of resistance for the sensor, and $\overline{\Delta T(\tau)}$ is the calculated mean value of the temperature rise given by $\overline{\Delta T(\tau)}=P_0(\pi^{3/2}aK)^{-1}X(\tau)$, where a is the size of resistive sensor, P_0 is the total power applied to heat the sample, $X(\tau)$ is the modified Bessel function, and τ is the dimensionless parameter related to the transient measurement time t and the thermal diffusivity α via the expression $\tau=(t\alpha/a^2)^{1/2}$. Figure 4 presents a typical plot of the temperature rise in TPS measurements for NCD films on the Si substrate, as well as the temperature rise in the reference Si sample. Note that the rise for NCD film on the Si substrate was obtained for 0.1 W of the dissipated power, while that for the Si reference wafer was recorded for 0.9 W. The larger temperature rise for NCD films for a much smaller dissipated power illustrates the difference in thermal resistance between these two samples.

IV. RESULTS AND DISCUSSION

First, we discuss the results of the measurements carried out by using the 3ω method. Figure 5 presents thermal conductivity K as a function of temperature for the UNCD film with 25% of N_2 (marked by squares). For comparison, it also shows the thermal conductivities of the undoped UNCD film (marked by triangles) and MCD film (marked by circles). The first observation is that the measured K values for UNCD are much smaller than those for the crystalline diamond or MCD films. For the UNCD without added nitrogen, the RT thermal conductivity is $K=16.6$ W/m K, while for the nitrogenated UNCD, the RT thermal conductivity further reduces to 8.6 W/m K in the film with 25% N_2 addition. The reduction with the increased N_2 concentration is similar to what is observed in bulk crystalline semiconductors due to the stronger phonon scattering on point defects.[43] However, in our case, the thermal conductivity reduction may also come from the grain boundary modifications caused by the presence of nitrogen. The measured RT thermal conductivity of the MCD sample is $K=551$ W/m K, which is two to four times smaller than that for crystalline diamond but still much

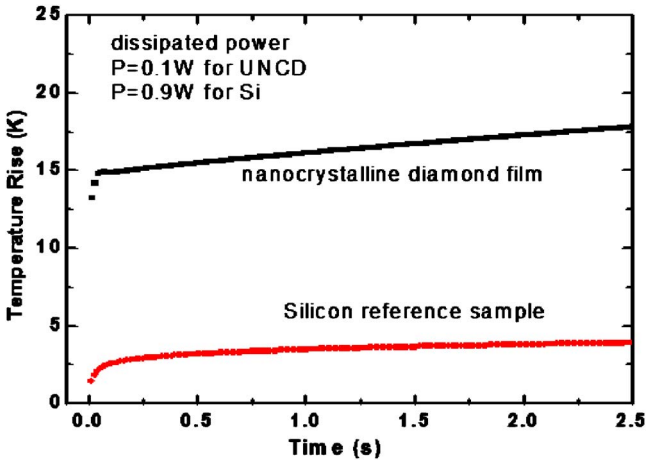

FIG. 4. (Color online) Transient temperature rise for the UNCD film on the Si substrate and reference Si sample measured by the TPS technique.

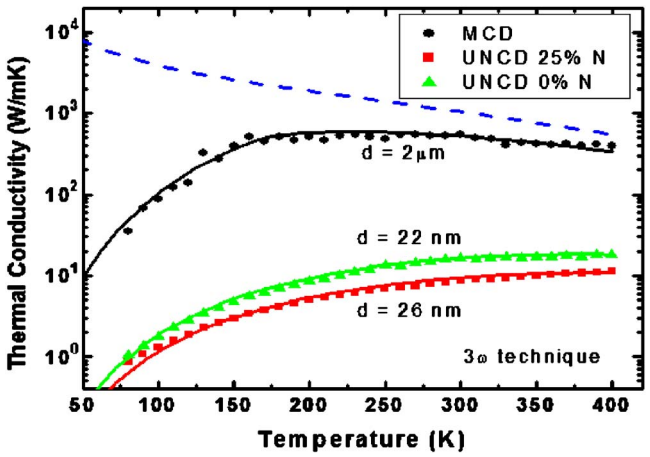

FIG. 5. (Color online) Thermal conductivities as a function of temperature measured for MCD and the "undoped" and nitrogenated UNCD films. The solid lines are simulation results obtained by using the PHM. The dashed line represents the bulk thermal conductivity obtained by the Klemens–Callaway approach. The solid symbols represent the measured values of thermal conductivity measured by the 3ω technique for the temperature range of 80–400 K.

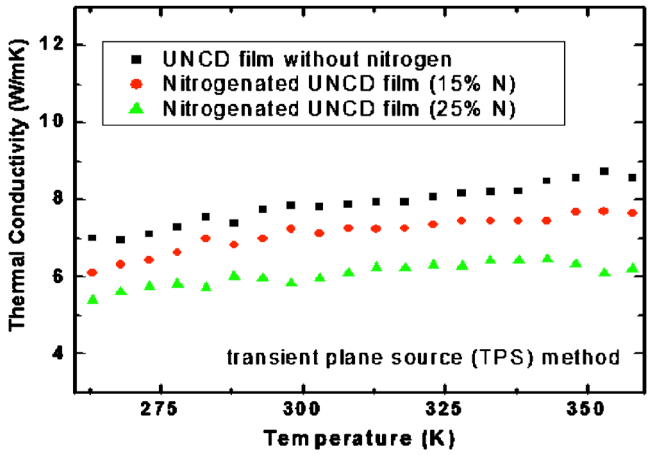

FIG. 6. (Color online) Thermal conductivity as a function of temperature for the UNCD samples measured by the transient plane technique.

higher than the thermal conductivity of Si (~145 W/m K at RT). The solid and dashed lines in Fig. 5 are the results of the calculations, which are discussed below.

Unlike the high quality bulk diamond single crystals and polycrystalline diamond, which show a peak in K vs T dependence typically in the range of $T=50-150$ K (the peak shifts to higher temperatures for more defective diamonds), the UNCD and MCD films do not manifest a pronounced low-temperature maximum. The thermal conductivity of MCD shows a flattened peak $K=550$ W/cm K at ~150 K and rolls off slower than $1/T$ near RT. The $1/T$ decrease is characteristic of low-defect bulk crystals at high temperatures and is related to the anharmonic umklapp phonon-phonon interaction. For a large variety of polycrystalline CVD films that greatly differed in quality, a general relationship $K\sim 1/T^x$ above RT was established[18] with the exponent x ranging within $0.17<x<1.02$. The smaller x values correspond to more defective films. The phonon scattering from the grain boundaries plays an important role at low T.[19,45,46]

The temperature dependence of the thermal conductivity of the UNCD samples is completely different from that of the bulk crystals and MCD film. It does not have a maximum and monotonically increases with T. The K values extracted from the 3ω measurements can be approximated as $K=AT^{\gamma}$ near RT (260–360 K), where $A\approx 1.8\times 10^{-4}$ W/m K and $\gamma=1.1$ for the nitrogenated UNCD film (25% of N_2) and $A\approx 4.32\times 10^{-3}$ W/m K and $\gamma=0.6$ for the UNCD film without nitrogen addition. The monotonic K increase with temperature is similar to that in the disordered materials. It is interesting to note that the 25% nitrogenation of an NCD film causes an ~50% drop in its RT thermal conductivity. The latter may have important consequences for the proposed electronic application of diamond materials.[14,15]

We measured the thermal conductivity of the same set of UNCD samples by using the TPS technique. First, the instrument and sensor calibrations were verified by measuring the thermal conductivity of a reference Si wafer. The RT value for Si has been determined to be 149 W/m K, which is very close to the tabulated value. Figure 6 shows the thermal conductivities of the UNCD films on Si with and without nitrogen addition, which were measured by using the hot disk method in the T range from 260 to 360 K. The RT values for the undoped, 15%, and 25% nitrogenated UNCD films were determined to be 7.8, 7.2, and 5.8 W/m K, respectively. One can see again that the increase in the N_2 concentration results in smaller values of the thermal conductivity. The results obtained by the TPS technique are in reasonable agreement with the K values measured by the 3ω method. The discrepancy between the thermal conductivities obtained by two different techniques for the nitrogenated UNCD (25% of N2) is about 25%, which is a rather typical deviation for different experimental techniques. The lower values of the thermal conductivity that were obtained with the TPS technique can be explained by the larger thermal contact resistance between the sensor and the film under study compared to the thermal boundary resistance associated with the interface between the metal heater thermometer and the film in the 3ω method. The K values extracted from the TPS measurements can also be approximated as $K=AT^{\gamma}$ near RT, where $A\approx 0.18$ W/m K and $\gamma=0.6$ for the nitrogenated UNCD film (15% of N_2) and $A\approx 0.14$ W/m K and $\gamma=0.7$ for the NCD film without N_2 addition.

We have analyzed the thermal conductivity of NCD and MCD material systems with the phonon-hopping model (PHM) proposed by Braginsky *et al.*[25] for polycrystalline materials. The PHM assumes that the phonon transport inside the grain follows the "bulk rules" while the phonon transition, i.e., hopping, from one grain to another through the intergrain boundary is governed by the semiempirical boundary transparency parameter t. The PHM thermal conductivity is written as[25]

$$K = k_B T \int_0^{\theta_D/T} \frac{K_i F(x) t \bar{S} \Phi}{\hbar k_B^{-1} K_i a^2 d + k_B \theta_D F(x) t \bar{S} \Phi} dx, \tag{1}$$

where

$$F(x) = \frac{9}{2}\left(\frac{T}{\theta_D}\right)^4 \frac{x^4 e^x}{(e^x-1)^2}\left(x-\frac{\theta_D}{T}\right)^2. \tag{2}$$

Here, θ_D is the Debye temperature, a is the lattice constant, d is the average grain size, $\bar{S}$ ($\approx d^2$) is mean area of the intergrain boundary, $\hbar$ is the Planck constant, k_B is the Boltzmann constant, Φ is the grain size fluctuation factor, and K_i is the inside-grain "bulk" thermal conductivity given by

$$K_i = \tfrac{1}{3} C_V V_G \Lambda, \tag{3}$$

where C_V is the heat capacity, V_G is the average phonon group velocity, and Λ is the bulk phonon mean free path (MFP).

In the model of Braginsky *et al.*,[25] Λ is expressed through the melting temperature T_m and Gruneisen parameter γ as $\Lambda=(20T_m a)/\gamma^2 T)$. We modified the analysis by explicitly calculating the phonon MFP using the Klemens–Callaway approach, where it is defined as[47]

$$\Lambda = (1/\Lambda_B + 1/\Lambda_R + 1/\Lambda_U)^{-1} + \lambda/2. \tag{4}$$

Here, $1/\Lambda_B=A^{-1}$ is the phonon-boundary scattering term, $1/\Lambda_R=B/\lambda^4$ is the point-defect Rayleigh scattering term, $1/\Lambda_U=CTe^{-D/T}/\lambda^2$ is the three-phonon umklapp scattering term, $\lambda=\hbar V_S/k_B T$ is the acoustic phonon wavelength, V_S is

TABLE I. Scattering parameters for the MCD and UNCD films.

Film type	B (cm^3)	C (cm/K)	D (K)
MCD	0.6×10^{-31}	1×10^{-14}	1250
UNCD (no N_2)	7.5×10^{-31}	2×10^{-14}	650
UNCD (with N_2)	7.0×10^{-31}	3×10^{-14}	650

the sound velocity, and A, B, C, and D are the material related constants. The material related constants are obtained by comparison to the experimental data.[47] Table I lists the values extracted for our samples. The value of B increases with the nitrogenation due to the stronger impurity mass-difference scattering on N atoms, which is assumed to incorporate both inside the grain and on the grain boundaries. One should note that at a low temperature, MFP is large and scattering on the grain boundaries becomes significant.[48] The boundary scattering term $1/\Lambda_B$ in Eq. (4), which describes the acoustic phonon scattering on the rough boundaries of the film, does not strongly influence the thermal resistance of UNCD films since the phonon scattering on the grain boundaries is by far the dominant relaxation mechanism. In the low-T regime, the thermal conductivity is defined by the grain size d and can be evaluated from the expression[49] $K_i=(1/3)C_V V_G d$.

The phonon-hopping parameter t is obtained from fitting to the experimental data, although in some simplest cases, it can be calculated from the first principles.[25,50] The best-fit PHM curves for the reference UNCD ($d=22$ nm) and MCD ($d=2$ μm) were obtained with $t=0.52$ and $t=0.9$, respectively, while the best-fit curve for the 25% nitrogenated NCD ($d=26$ nm) was calculated with $t=0.24$ (see Fig. 6). One can see excellent agreement between the theory and experiment for UNCD films for the whole examined temperature range from 80 to 400 K. The smaller t value for the nitrogenated NCD can be related to the fact that nitrogen atoms cluster on the grain boundaries, as reported for similar materials in Ref. 13. The accumulation of the nitrogen atoms on the grain boundaries and the increased thickness of the grain boundaries composed of nondiamond carbon[51] reduce the intergrain transparency and the thermal conductivity of NCD. It is interesting to note that the effect of the nitrogen clustering on the thermal conductivity can be partially offset by the increase in the grain size as a result of nitrogenation. It was observed earlier that the addition of N_2 leads to a larger grain size.[13,51] The larger grain size results in a lesser number of grain boundaries and, hence, a smaller thermal resistance of the whole film.

We also analyzed the upper and low bounds of the thermal conductivity in carbon materials with two other theoretical models in order to verify their consistency with the PHM results. The dashed curve in Fig. 5 is calculated for bulk crystalline diamond by using the standard Callaway–Klemens approach.[49,52] The calculation procedure is analogous to the one that some of us reported elsewhere for another material system.[53] This curve presents the upper bound for the thermal conductivity, which can be obtained in a diamond-type material without boundary effects on the acoustic phonons. One can see that the K values for MCD are relatively close to the upper bound near RT but much smaller at low T where, in addition to the thermal resistance of the grain boundaries, the thermal resistance of the film interfaces starts to play a role. The low bound for the thermal conductivity in carbon-based materials can be evaluated from the minimum thermal conductivity (MTC) model proposed by Cahill and Pohl[54] for the amorphous and disordered materials. The values calculated with MTC are about an order of magnitude lower than the measured thermal conductivity for the UNCD films shown in Fig. 5. The latter indicates that the sp^3 phase ordering inside the grains, even if they are of nanometer size, leads to a strong increase in the thermal conductivity compared to the that of amorphous carbon.

It is illustrative to compare the thermal conductivity of UNCD films with that of diamondlike carbons. Table II summarizes the RT values for UNCD films measured by two different experimental techniques together with the K values reported in literature for DLC films. The thermal conductivity of UNCD is more than four times higher than that for the DLC samples with the highest sp^3 phase content, such as ta-C. Note that although the difference between the net sp^3

TABLE II. Thermal conductivities of UNCD and diamondlike carbon.

Film type	Film thickness	Deposition process	K (W/mK)	Method	Comments	Source
UNCD: no N_2	2.17 μm	PECVD	16.6	3ω	Grain size $d=22$ nm	This work
UNCD: with 25% N_2	9.54 μm	MPCVD	8.6	3ω	Grain size $d=26$ nm	This work
MCD	3.4 μm	MPCVD	551.0	3ω	Grain size $d=2$ μm	This work
UNCD: no N_2	2.17 μm	PECVD	7.8	TPS	Grain size $d=22$ nm	This work
UNCD: with 15% N_2	8.90 μm	MPCVD	7.2	TPS	Grain size $d=17$ nm	This work
UNCD: with 25% N_2	9.54 μm	MPCVD	5.8	TPS	Grain size $d=26$ nm	This work
ta-C	70 nm	FCVA	3.5	3ω	Amorphous sp^3 phase	Ref. 23
ta-C:H	70 nm	ECWR	1.3	3ω	28% H_2	Ref. 23
DLCH	85 nm	PECVD	0.7	3ω	Anisotropic sp^2 and sp^3	Ref. 23
GLCH	52 nm	Sputtering	0.4	3ω	18% H_2	Ref. 23
PLCH	94 nm	PECVD	0.3	3ω	36% H_2	Ref. 23
ta-C	20–100 nm	FCVA	4.7	Photothermal		Ref. 55
UNCD	16 μm	CVD	26	3ω		Ref. 21

contents of UNCD and ta-C is small, the sp^3 phase inside the UNCD grains is ordered, while in ta-C, it is amorphous. Thus, the ordering of the sp^3 phase leads to an increase in the thermal conductivity.[24] The grain boundaries in UNCD films may also strongly affect thermal conduction. Recent reports suggested that under certain growth conditions, the presence of N_2 in a high amount of process gas can dramatically change the geometry of UNCD grains and can lead to the formation of diamond nanowires.[56,57] If the nanowires are aligned, one can expect an anisotropic thermal conductivity in these nanostructures. Such anisotropic thermal conductivity was observed in thick MCD films with a columnar grain structure.[55] The small thermal conductivity of UNCD is in sharp contrast to that of crystalline diamond[17–20] and the recently discovered extremely high thermal conductivity of graphene,[58] which exceeds that of carbon nanotubes.[59]

V. CONCLUSION

We investigated the thermal conductivity of nitrogenated nanocrystalline diamond films on silicon and compared the measured results to the theoretical predictions. In order to minimize the experimental uncertainty, we used two different measurement techniques: the 3ω method and TPS method. Both techniques gave consistent values of the thermal conductivity over the examined temperature ranges. It was shown that the temperature dependence of the thermal conductivity of UNCD films can be adequately described by the PHM. The RT thermal conductivity of UNCD is 8.6–16.6 W/m K and decreases with the addition of nitrogen, which is used to form a *n*-type semiconductor. The obtained results shed light on the nature of thermal conduction in partially disordered nanostructured materials. They can also be used for estimating the thermal resistance of the electrically conducting UNCD and MCD films on silicon.

ACKNOWLEDGMENTS

The authors are thankful to A. Saveliev for the preparation of the NCD and MCD films and Dr. O. Lebedev for taking the SEM images. The work at UCR was supported, in part, by the DARPA-SRC funded FCRP Focus Center on Functional Engineered Nano Architectonics (FENA) and the National Science Foundation (NSF) award to A.A.B. The work at GPI was supported through the Program "New Materials and Structures" of the Physics Division of the Russian Academy of Sciences.

[1] C. E. Nebel, Nature (London) **2**, 431 (2003).
[2] J. A. Carlisle, Nature (London) **3**, 668 (2004).
[3] J. Griffin and P. C. Ray, Nanotechnology **17**, 1225 (2006).
[4] G. A. J. Amaratunga, Science **297**, 1657 (2002).
[5] E. Kohn, A. Denisenko, M. Kubovic, T. Zimmermann, O. A. Williams, and D. M. Gruen, Semicond. Sci. Technol. **21**, L32 (2006).
[6] D. M. Gruen, Annu. Rev. Mater. Sci. **29**, 211 (1999).
[7] W. Yang, O. Auciello, J. E. Butler, W. Cai, J. A. Carlisle, J. E. Gerbi, D. M. Gruen, T. Knickerbocker, T. L. Lasseter, J. N. Russell, J. M. Smith, and R. J. Hamers, Nat. Mater. **1**, 253 (2002).
[8] O. A. Williams, Semicond. Sci. Technol. **21**, R49 (2006).
[9] X. Xiao, J. Birrell, J. E. Gerbi, O. Auciello, and J. A. Carlisle, J. Appl. Phys. **96**, 2232 (2004).
[10] O. A. Williams, S. Curat, J. E. Gerbi, D. M. Gruen, and R. B. Jackman, Appl. Phys. Lett. **85**, 1680 (2004).
[11] S. Bhattacharyya, O. Auciello, J. Birrell, J. A. Carlisle, L. A. Curtiss, A. N. Goyette, D. M. Gruen, A. R. Krauss, J. Schlueter, A. Sumant, and P. Zapol, Appl. Phys. Lett. **79**, 1443 (2001).
[12] T. Zimmermann, M. Kubovic, A. Denisenko, K. Janioschowsky, O. A. Williams, D. M. Gruen, and E. Kohn, Diamond Relat. Mater. **14**, 416 (2005).
[13] J. E. Gerbi, O. Auciello, J. Birrell, D. M. Gruen, B. W. Alphenaar, and J. A. Carlisle, Appl. Phys. Lett. **83**, 2001 (2003).
[14] Z. Di, P. K. Chu, M. Zhu, R. K. Y. Fu, S. Luo, L. Shao, M. Nastasi, P. Chen, T. L. Alford, J. W. Mayer, M. Zhang, W. Liu, Z. Song, and C. Lin, Appl. Phys. Lett. **88**, 142108 (2006).
[15] G. Aichmayr, A. Avellan, G. S. Duesberg, F. Kreupl, S. Kudelka, M. Liebau, A. Orth, A. Sanger, J. Schumann, and O. Storbeck, IEEE Symposium on VLSI Technology, Vols. 12–14, 2007 (unpublished), p. 186.
[16] O. Auciello, S. Pacheco, A. V. Sumant, C. Gudeman, S. Sampath, A. Datta, R. W. Carpick, V. P. Adiga, P. Zurcher, Z. Ma, H. C. Yuan, J. A. Carlisle, B. Kabius, J. Hiller, and S. Srinivasan, IEEE Microw. Mag. **8**, 61 (2007).
[17] R. Berman, P. R. W. Hudson, and M. Martinez, J. Phys. C **8**, L430 (1975).
[18] A. V. Sukhadolau, E. V. Ivakin, V. G. Ralchenko, A. V. Khomich, A. V. Vlasov, and A. F. Popovich, Diamond Relat. Mater. **14**, 589 (2005).
[19] E. Wörner, C. Wild, W. Müller-Sebert, R. Locher, and P. Koidl, Diamond Relat. Mater. **5**, 688 (1996).
[20] J. E. Graebner, J. A. Mucha, L. Seibles, and G. W. Kammlott, J. Appl. Phys. **71**, 3143 (1992).
[21] M. A. Angadi, T. Watanabe, A. Bodapati, X. Xiao, and O. Auciello, J. A. Carlisle, J. A. Eastman, P. Keblinski, P. K. Schelling, and S. R. Phillpot, J. Appl. Phys. **99**, 114301 (2006).
[22] S. Ahmed, R. Liske, T. Wunderer, M. Leonhardt, R. Ziervogel, C. Fansler, T. Grotjohn, J. Asmussen, and T. Schuelke, Diamond Relat. Mater. **15**, 389 (2006).
[23] W. L. Liu, M. Shamsa, I. Calizo, A. A. Balandin, V. Ralchenko, A. Popovich, and A. Saveliev, Appl. Phys. Lett. **89**, 171915 (2006).
[24] M. Shamsa, W. L. Liu, A. A. Balandin, C. Casiraghi, W. I. Milne, and A. C. Ferrari, Appl. Phys. Lett. **89**, 161921 (2006).
[25] L. Braginsky, N. Lukzen, V. Shklover, and H. Hofmann, Phys. Rev. B **66**, 134203 (2002).
[26] E. Loubnin (unpublished).
[27] W. L. Hsu, D. M. Tung, E. A. Fuchs, K. F. McCarty, A. Joshi, and R. Nimmagadda, Appl. Phys. Lett. **55**, 2739 (1989).
[28] G. Z. Wang, F. Ye, C. Chang, Y. Liao, and R. C. Fang, Diamond and Relat. Mater. **9**, 1712 (2000).
[29] F. Tuinstra and J. L. Koenig, J. Chem. Phys. **53**, 1126 (1970).
[30] R. P. Vidano, D. B. Fischbach, L. J. Willis, and T. M. Loehr, Solid State Commun. **39**, 341 (1981).
[31] A. C. Ferrari and J. Robertson, Philos. Trans. R. Soc. London, Ser. A **363**, 2477 (2004).
[32] A. C. Ferrari and J. Robertson, Phys. Rev. B **63**, 121405 (2001).
[33] J. Birrell, J. E. Gerbi, O. Auciello, J. M. Gibson, J. Johnson, and J. A. Carlisle, Diamond Relat. Mater. **14**, 86 (2005).
[34] X. Xiao, J. Birrell, J. E. Gerbi, O. Auciello, and J. A. Carlisle, J. Appl. Phys. **96**, 2232 (2004).
[35] J. Griffin and P. C. Ray, Nanotechnology **17**, 1225 (2006).
[36] A. C. Ferrari, S. E. Rodil, and J. Robertson, Phys. Rev. B **67**, 155306 (2003).
[37] I. I. Vlasov, V. G. Ralchenko, E. Goovaerts, A. V. Saveliev, and M. V. Kanzyuba, Phys. Status Solidi A **203**, 3028 (2006)
[38] I. I. Vlasov, E. Goovaerts, V. G. Ralchenko, V. I. Konov, A. V. Khomich, and M. V. Kanzyuba, Diamond Relat. Mater. **16**, 2074 (2007).
[39] D. G. Cahill, Rev. Sci. Instrum. **61**, 802 (1990).
[40] D. G. Cahill and R. O. Pohl, Phys. Rev. B **35**, 4067 (1987).
[41] V. Ralchenko, S. Pimenov, V. Konov, A. Khomich, A. Saveliev, A. Popovich, I. Vlasov, E. Zavedeev, A. Bozhko, E. Loubnin, and R. Khmelnitskii, Diamond Relat. Mater. **16**, 2067 (2007).
[42] W. L. Liu and A. A. Balandin, Appl. Phys. Lett. **85**, 5230 (2004); W. L. Liu and A. A. Balandin, J. Appl. Phys. **97**, 073710 (2005).
[43] M. Shamsa, W. L. Liu, A. A. Balandin, and J. L. Liu, Appl. Phys. Lett. **87**, 202105 (2005).
[44] S. E. Gustafsson, Rev. Sci. Instrum. **62**, 797 (1991); M. Gustavsson, E. Karawacki, and S. E. Gustafsson, *ibid.* **65**, 3856 (1994).
[45] J. E. Graebner, M. E. Reiss, L. Seibles, T. M. Hartnett, R. P. Miller, and C. J. Robinson, Phys. Rev. B **50**, 3702 (1994).
[46] J. E. Graebner, J. A. Mucha, and F. A. Baiocchi, Diamond Relat. Mater. **5**, 682 (1996).

[47]J. R. Olson and R. O. Pohl, J. W. Vandersande, A. Zolton, T. R. Anthony, and W. F. Banholzer, Phys. Rev. B **47**, 14850 (1993).
[48]J. E. Graebner, J. Wide Bandgap Mater. **7**, 105 (1999).
[49]P. G. Klemens, in *Solid State Physics*, edited by F. Seitz and D. Turnbull (Academic, New York, 1958), Vol. 7.
[50]L. Braginsky, V. Shklover, H. Hofmann, and P. Bowen, Phys. Rev. B **70**, 134201 (2004).
[51]J. Birrell, J. A. Carlisle, O. Auciello, D. M. Gruen, and J. M. Gibson, Appl. Phys. Lett. **81**, 2235 (2002).
[52]J. Callaway, Phys. Rev. B **113**, 1046 (1959).
[53]J. Zou, D. Kotchetkov, A. A. Balandin, D. I. Florescu, and F. H. Pollak, J. Appl. Phys. **92**, 2534 (2002); D. Kotchetkov, J. Zou, A. A. Balandin, D. I. Florescu, and F. H. Pollak, Appl. Phys. Lett. **79**, 4316 (2001).
[54]D. G. Cahill and R. O. Pohl, Solid State Commun. **70**, 927 (1989).
[55]J. E. Graebner, S. Jim, G. W. Kammlott, J. A. Herb, and C. F. Gardinier, Nature (London) **359**, 401 (1992).
[56]R. Arenal, P. Bruno, D. J. Miller, M. Bleuel, J. Lal, and D. M. Gruen, Phys. Rev. B **75**, 195431 (2007).
[57]I. I. Vlasov, O. I. Lebedev, V. G. Ralchenko, E. Goovaerts, G. Bertoni, G. van Tendeloo, and V. I. Konov, Adv. Mater. (Weinheim, Ger.) **19**, 4058 (2007).
[58]A. A. Balandin, S. Ghosh, W. Bao, I. Calizo, D. Teweldebrhan, F. Miao, and C. N. Lau, Nano Lett. 8, 902 (2008).
[59]G. Chen, P. Hui, and S. Xu, Thin Solid Films **366**, 95 (2000).